An Experimental and Numerical Study on A Paddle-type Breakwater

Xuefeng Han [1], Longzhi Han [2], Baiyu Chen [3], Chunpeng Liu [4], Yunfeng Chen [5]

[1] School of Economics and Management, Harbin Engineering University, Harbin, China
[2] Qingdao Haida Haiyang Gongcheng Company Limited, Qingdao, China
[3] College of Engineering, University of California Berkeley, Berkeley, CA, USA
[4] College of Engineering, Ocean University of China, Qingdao, 266100, China
[5] Qingdao West Coast Cultural Industry Investment Co., Ltd, China

Abstract: An effective design of breakwaters is very important for protecting the engineering infrastructures as well as natural reserves within the coastal area. Meanwhile, the daily operation and maintenance of a harbour also requires the breakwater as a good shelter. In this paper, a new type active breakwater is proposed, which suppresses the incident waves by generating a steady surface flow through the movement of the paddles along wave crest direction. Both experiments in physical wave tank and numerical simulations are carried out to investigate the performance of the device and the results confirm that the device is very effective for absorbing incident waves. Meanwhile, it is found that the absorbing coefficient is strongly associated with the rotate speed of the paddle and the incoming wave length. In addition, comparison with the bubble breakwater is also made, and the proposed device is observed to exhibit a superior efficiency. The study provides a useful reference for engineering practices by using such a design, and may motivate further study to improve the model in the future.

Keywords: numerical simulation; physical modelling; wave breaker; coastal engineering

1. Introduction

Over the last few decades, globalization has driven fast growing international trade and increasingly demands of large cargo ship. As a consequence, deep water harbours are constructed to adapt to the rapidly changing situation. However, those harbours are always constructed in deep open seas and are more easily affected by the incoming waves, compared with that in the shallow waters. Thus, effective design of the breakwater is urgently required to provide good protections for these harbours in deep water. However, the traditional vertical-type and slope-type breakwater, which are originally designed for shallow water harbours, cannot meet the requirements, due to the difficulties and high cost of construction and maintenance, etc. Therefore, new designs of breakwater, e.g., open-type, are becoming more and more popular in engineering practices [1-5].

Compare with the traditional breakwaters, the open-type designs are less expensive and easier to construct, while can effectively absorbing incident waves, thus have attracted extensive attentions from communities of both engineers and applied scientists. New ideas of the designs have been suggested, e.g., vertical thin barrier [6-8], submerged plate [9-11], twin plate [12-14], T-type [15-18] even n-type [18-21], etc. Note that such kind of breakwater can be categorized as the passive breakwater, same with the traditional vertical type and slope type designs, which means the structure is fixed and provided as an obstacle to restrict the wave motion.

Nevertheless, the study on the active breakwater is rare, at least in the public domain. One well-known example is the bubble breakwater, which dissipates the waves by generating a horizontal current near free surface via producing large amount of bubbles from the pipe lying on the seabed. The absorbing efficiency largely relies on the volume of air supplies, and relevant studies can be found in [22-26]. However, due to that the active breakwater has a high demand of electricity, very few of them are used in real practices [27-29]. However, studies on wave energy convertor have received lots of attentions more recently, which can be seen as an alternative solution to resolve the electricity demand for the active breakwater [30-35].

In this paper, a new type of the active breakwater is proposed. Its performance, i.e., the absorbing efficiency, is explored through both physical tank experiments and numerical simulations. The effectiveness of the new device is demonstrated and the results look promising. This study provides a good reference for further development of the active breakwater in order to offer more efficient coastal protections.

2. Description of the Breakwater

According to the linear wave theory, the water particles move in a circle or elliptic, and decay exponentially along the water depth. Therefore, the amount of water within 2 ~ 3 wave lengths beneath the free surface contains nearly 90% ~ 98% of the total wave energy. Based on that, we introduce a new device similar to the bubble breakwater, which can generate a horizontal crestwise current near the free surface by using paddles, so that the waves can be suppressed. By using this idea, two models are proposed and their efficiency are investigated.

2.1. Model 1: Chain-mounted Paddle

The sketch of model 1 is shown in Fig. 1, where the dimension of the frame is 2.26m x 0.52m x 0.3m. A total of 12 paddles are mounted on two individual chains, and are driven by the motor through the transmission belt. An illustration of the movement of the paddles is shown in Fig. 2, where one group of the paddles move in close wise direction and the other in anticlockwise direction. By doing so, a horizontal shear current is generated from the center of the frame and move to the ends in two different directions.

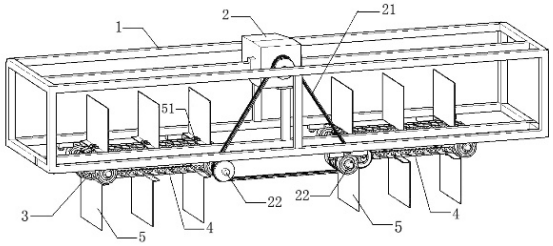

Figure 1. Sketch of Model 1 (1 Frame, 2 Motor, 21 Transmission belt, 3 Chain wheel, 4 Chain, 5 Paddle).

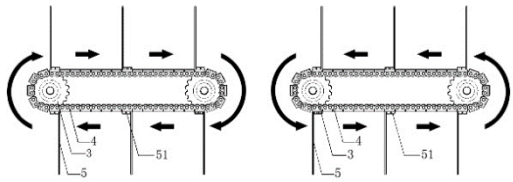

Figure 2. Illustration of the motion of the paddles.

2.2. Model 2: Spindle-mounted Paddle

The sketch of Model 2 is shown in Fig. 3, where the size of the frame is the same with Model 1. However, the difference is that the paddle is now mounted on the spindle, instead of the chain as in Model 1. Therefore, the paddles of Model 2 rotate about the spindle center, whereas that of Model 1 shift horizontally.

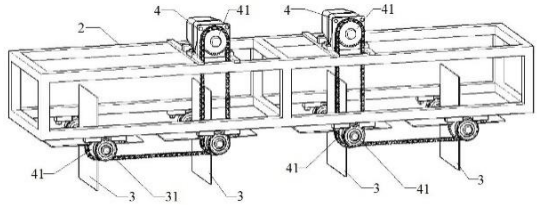

Figure 3. Sketch of Model 2 (2 Frame, 3 Paddle, 31 Spindle, 4 Motor, 41 Chain wheel).

3. Methodologies

3.1. Experiments in Physical Flume/Tank

The physical experiments on Model 1 and 2 are performed in the wave flume and tank in the laboratory in Ocean University of China, respectively. The flume is 40m in length and 3m in width, with water depth d = 1 m. Porous materials are placed at the end of the flume to reduce the effects of the reflected waves. The side and plan views of the experiment set-up are shown in Fig. 4, where the device, i.e., Model 1, is installed at 23m away from the wave maker. The submerge depth of the paddle is 0.08 m in still water. A in-situ picture of Model 1 at working in the flume during testing is shown in Fig. 5. Two wave gauges are mounted 1m away from the device at the upstream and downstream, respectively, and the recorded time history will be used to estimate the absorbing coefficient of the device. The absorbing coefficient is estimated by using the formula

$$C_w = \frac{H_0 - H_1}{H_0} \times 100\% \quad (1)$$

where H_0 and H_1 are wave heights measured at gauge 1# and 2#, respectively.

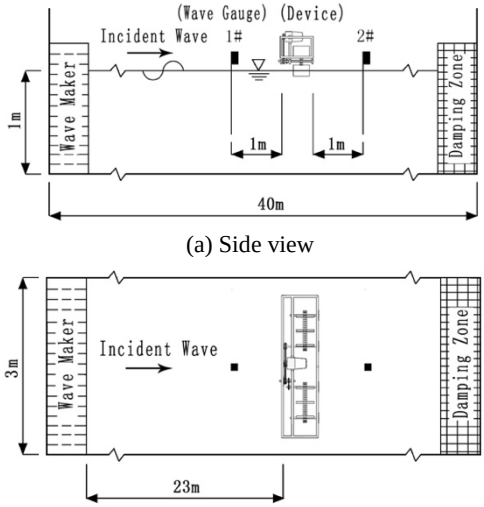

Figure 4. Experimental set-up in the wave flume for Model 1.

Figure 5. Photograph of Model 1 in wave flume.

Meanwhile, the experiment on Model 2 is carried out in the wave tank, of which the dimension is 40m x 30m and water depth d = 1.015m. The experiment set-up shows that the device, i.e., Model 2, is 23m away from the wave maker, where the submerged depth of the paddle is 0.0915m. Two wave gauges are installed similar to the tests on Model 1 to measure the wave height in order to estimate the absorbing coefficient. A photograph of Model 2 during test in the wave tank is also provided in Fig. 6.

Figure 6. Photograph of Model 2 in wave tank.

3.2. Numerical Simulations

The numerical simulations are performed by using the commercial software Flow-3D, which is widely used for modelling wave-structure interactions. The software solves the coupled continuity equation and unsteady Reynolds-Averaged Navier-Stokes equation, where the RNG k — turbulent model is chosen in this study. Based on the Volume-Of-Fluid (VOF) technique, the software uses the improved inhouse TruVOF method to track the free surface, while the fluid-structure interaction is modelled by using its General Moving Object (GMO) module. The details of the software can be found in the user manual, so are omitted here for brevity, as the focus of this study is not on the numerical method itself. The effectiveness of the software for modelling the wave-paddle interactions will be shown later in this paper.

The dimension of the numerical wave tank (NWT) is the same with the physical flume, i.e., 40m x 3m, with water depth of 1m. Structured orthogonal mesh strategy is used, and the configuration of the mesh is shown in Table 1, where the NWT is divided into 2 blocks and difference mesh sizes are used. The device is put in block 1 where the mesh is finer for better accuracy, and block 2 is used for wave damping to avoid reflection.

Inlet boundary condition is used to generate waves, where the linear wave theory is employed. However, the distance between the inlet boundary and the device is 3 meters, which is sufficient for waves to relax and build up nonlinearities. A snapshot of the numerical modelling can be found in Fig. 7.

Table 1. Configuration of the mesh.

Block No.	x(m)	Mesh size(m)
1	0-5	0.04x0.04x0.04
2	5-40	0.08x0.08x0.08

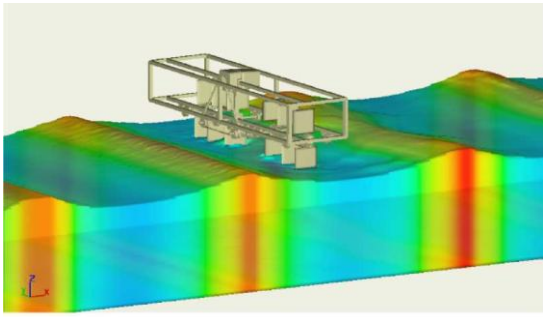

Figure 7. Snapshot of the numerical modelling

4. Results and Discussions

4.1. Validation of the Numerical Model

Firstly, the numerical model is validated by comparing its results with the experiment results of Model 1 in the flume. Regular waves with period of 1s and three different height, i.e., 13cm, 15cm and 16cm, are generated, and the rotating speed of the paddle is 57 rpm/min. The estimated absorbing coefficients for both the experiments and numerical simulations are presented in Table 2 while the comparison of the wave heights recorded at the gauges are shown in Fig. 8. Good agreement between the experiment and the numerical simulation is observed, which implies that the configuration of the numerical simulation gives satisfactory results and can be used in the following analysis.

Furthermore, to validate the numerical simulation for evaluating Model 2 in the wave tank, the width of the NWT is extended to 9 m, in order to minimize the effects of the sidewalls. Same mesh configuration as in Table 1 is adopted. Regular waves of height 16cm, period 1.25s are generated, and the rotating speed of the paddle is 90rpm/min. The free surface time histories at the wave gauges in both the physical and numerical wave tank showed that the free surface in the numerical simulation agrees very well with the experiment. It means that results given by the numerical simulation for Model 2 are reliable by using the current configurations.

Table 2. Comparison of the absorbing coefficients between the physical experiments and numerical simulation.

Cw (%)	H=0.13m	H=0.15m	H=0.16m
Flume	25.6	29.1	28.2
Flow — 3D	32.9	33.0	29.6

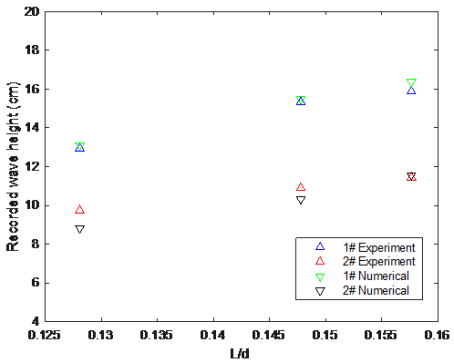

Figure 8. Comparison of the wave heights.

4.2. Comparison between Model 1&2

In this subsection, the absorbing coefficients of Model 1 and 2 are compared in order to identify which design is more efficient. The results obtained by numerical simulations are presented in Table 3, in which it can be found that the absorbing coefficients of Model 2 is larger than the Model 1, which implies that Model 2 outperforms Model 1 for absorbing incident waves based on the tested cases. The reason is that for the same rotating speed, the Model 2 is more efficient on producing the horizontal current. For example, the maximum velocity of the water particle normal to the paddle can be expressed as

$$U_{max} = n \times R_{1,2} \quad (2)$$

where R1 and R2 are the radius of the chain wheel for Model 1 and the length of the paddle for Model 2, respectively. It is obvious that Ri < R2, which indicates that the maximum water particle velocity generated by Model 1 is less than that by Model 2. Therefore, Model 2 is shown to be a more efficient design over Model 1 and only the efficiency of Model 2 will be further explored in this study.

Table 3. Comparison of the absorbing coefficient between Model 1&2.

Cw (%)	H=0.13m	H=0.15m	H=0.16m

Model 1	32.9	33.0	29.6
Model 2	35.8	36.2	35.0

Table 4. Working conditions.

No.	Wave height H(m)	Wave period T(s)	Wave length L(m)	Rotating speed n (r/min)
1	0.15	1	1.56	69,90,120
2	0.16	1.25	2.41	69,90,120
3	0.125	1.5	3.36	69,90,120
4	0.14	1	1.56	90
5	0.13	1	1.56	90

Table 5. Efects of wave steepness on the absorbing coefficients.

H/L	Cw (%)
0.0962	50.5
0.0898	51.5
0.0834	49.5

4.3. Further Experiments on Model 2

In this subsection, the absorbing efficiency of Model 2 will be further investigated by testing on different wave conditions with different rotating speeds of the paddles. The cases to be tested are summarized in Table 4. The effects of wave steepness, wave length and the rotating speed of the paddle on the absorbing coefficient will be explored. Note that the results in this subsection is obtained by performing the experiments in the physical wave tank only.

4.3.1. Effects of wave steepness

The magnitude of the wave steepness represents the degree of nonlinearities of the incident waves. Higher steepness waves exhibit stronger nonlinearities. For regular waves, nonlinearities mainly affect the vertical asymmetry of the wave profile, which can elevate the wave crest and flatten the trough. To investigate the effects of wave steepness, i.e., the asymmetry feature of higher steepness waves, experiments are carried out where other parameters are kept the same, e.g., water depth 1.015m, rotating speed 90 r/min. The estimated absorbing coefficient is shown in Table 5. It is found that the absorbing coefficient does not vary too much when the wave steepness is changed, which indicates that the effect of the wave steepness, i.e., nonlinearities, on the absorbing coefficient of the device is insignificant.

4.3.2. Effects of wave length and rotating speed

Experiments are then carried out in the wave tanks to investigate the effects of wave length and the rotating speed of the paddles. Results of the absorbing coefficients are presented in Table 6. It shows in the table that the absorbing coefficients vary significantly when the wave length and rotating speed are changed, which means that the efficiency of Model 2 largely depends on those two factors. In addition, the results in the table indicate that:

a) For a fixed rotating speed, the absorbing coefficient increases when wave length becomes shorter;

b) For relatively shorter waves, larger rotating speeds gives better absorbing efficiency;

c) For relatively longer waves, the effects of the rotating speed on the absorbing coefficient is insignificant, which means that increasing the rotating speed cannot further improve the efficiency of the device.

Table 6. Effects of wave length and rotating speed Cw (%) on absorbing coefficient.

L/d	Cw (%)		
	n=69r/min	n=90r/min	n=120r/min
1.539	46.4	50.5	55.8
2.239	32.9	34.8	30.5
3.994	19.7	22.1	22.3

4.3.3. Discussion

The results in working conditions 1 to 3 are used to illustrate the relationship between the absorbing coefficient with the wave length and the rotating speed, where a surface is fitted to approximate the values of the absorbing coefficients in terms of the wave steepness and rotating speed. Additionally, the contour of the fitted surface is plotted in Fig. 9. Since the values of the absorbing coefficients in working condition 4 and 5 are not used to obtain the fitted surface, they can be used to validate the accuracy of the fitted surface. By extracting from the surface, the predicted absorbing coefficients for working condition 4 and 5 are 46.8% and 43.4%, of which the errors are 9.1% and 12.3%, respectively, comparing with the results obtained in the experiments. That means the approximated absorbing coefficient from the fitted surface can be used to accurately predict the efficiency of the device.

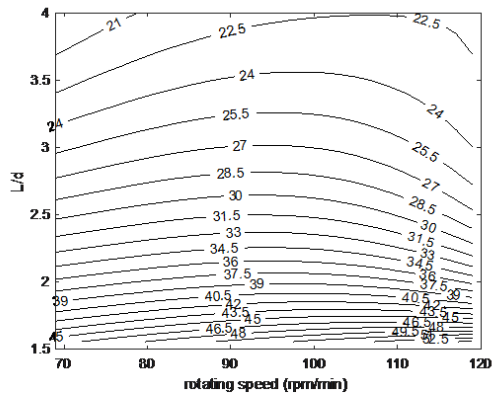

Figure 9. Contour of the absorbing coefficient.

5. Compare with Bubble Breakwater

Wang [1] studied the efficiency of a bubble breakwater and investigated the effects of the volumes of air supply, where the water depth is 0.8m and wave height 0.236m. It is found that for a fixed wave length, the bubble breakwater exhibits higher efficiency when the volume of air supply increases, while remains the same after the volume of air supply becomes larger than a certain value. Similarly, the absorbing coefficient of the proposed device, i.e, Model 2, increases if the rotating speed of the paddle becomes faster, while remain the same after the rotating speed exceeds a specific value. Thus, to make a comparison between the two different designs, only the highest efficiency that the breakwater can achieve is

compared. However, due to the limitations of the experiment facilities, using exact the same experiment conditions cannot be made. Nevertheless, the comparison of the highest absorbing coefficient between the two designs are presented in Fig. 10, in which it can be found that the proposed model outperforms the bubble breakwater in the overlapped zone of the wave length. As aforementioned, it is difficult to compare the efficiency of both the designs in the same range of the wave length due to the limitation of the experimental facilities. However, it is anticipated that the suggested device can achieve a higher efficiency than the bubble breakwater for relatively longer waves, since the submerged depth and the length of the paddle can also be adjusted. However, further study is needed to confirm that, but will not be discussed in this paper.

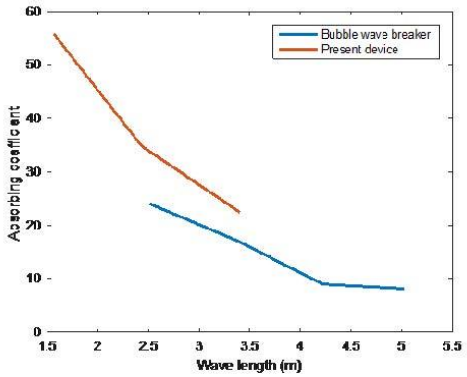

Figure 10. Comparison of the absorbing coefficient against wave length between paddletype and bubble breakwater

6. Conclusion

Two paddle-type breakwaters, i.e., a chain-mounted and a spindle-mounted device, are suggested in this study. The efficiency of the two devices are investigated through both physical experiments and numerical simulations. By comparing the absorbing efficiency, it is found that the latter is superior than the former for absorbing incident waves. By using the experimental data, the absorbing coefficient of the spindle-mounted device can be approximated if the wave length and the rotating speed of the paddle are known in advance. It provides a good reference for the current concept design to be further improved in the future, so that can be employed in engineering practices. Meanwhile, its efficiency is also compared with the bubble breakwater, and it is found that the suggested device outperforms the bubble breakwater for absorbing waves of same length. In the future, the effects of the length and submerged depth of the paddle will be investigated, while irregular waves should also be considered, both in uni-directional and spreading seas. Moreover, a new design in the future to use the wave motion to drive the paddles will be proposed and studied. In addition, there is also a necessary to carry out a systematic study to compare the new device with the bubble breakwater in the same working conditions.

Acknowledgments

The first author acknowledges the financial support from the National Natural Science Foundation of Shandong Province [No. ZR2019MEE050], the National Natural Science Foundation of China [No. 51379195], and the Graduate Education Foundation [No. HDYA19006].

References

[1] Wang, G. Investigation on the structure type and performance of the special breakwaters. Dalian: Dalian University of Technology.

[2] Wiegel, R.L. Transmission of wave past a rigid vertical thin barrier. J. Waterway, and Harbors Div., ASCE (1) (1960), pp. 1-12.

[3] Parsons, N.; Martin, P. Scattering of water waves by submerged plates using hypersingular integral equations. *Applied Ocean Research*, **1992**, vol. 14, no. 5, pp. 313-321.

[4] Koag, M.C.; Kou, Y.; Hala, O.S.; Lee, S. Transition-state destabilization reveals how human DNA polymerase β proceeds across the chemically unstable lesion N7-methylguanine. *Nucleic Acids Research*, **2014**, vol. 42, no. 13, pp. 8755-8766.

[5] Kou, Y.; Cheun, Y.; Koag, M.C.; Lee, S. Synthesis of 14',15'-dehydro-ritterazine Y via reductive and oxidative functionalizations of hecogenin acetate. *Steroids*, **2013**, vol. 78, no. 2, pp. 304-311.

[6] Kou, Y.; Koag, M.C.; Cheun, Y.; Shin, A.; Lee, S. Application of hypoiodite-mediated aminyl radical cyclization to synthesis of solasodine acetate. *Steroids*, **2012**, vol. 77, no. 11, pp. 1069-1074.

[7] Wen, R.; Umeano, A.C.; Kou, Y.; Xu, J.; and Farooqi A.A. Nanoparticle systems for cancer vaccine. *Nanomedicine*, **2019**, vol. 14, no. 5, pp. 627-648.

[8] Liu, G.; Chen, B.; Jiang, S.; Fu, H.; Wang, L.; Jiang, W. Double Entropy Joint Distribution Function and Its Application in Calculation of Design Wave Height. *Entropy*, **2019**, vol. 21, pp. 64.

[9] Liu, G., et al. Study on Threshold Selection Methods in Calculation of Ocean Environmental Design Parameters. *IEEE Access*, **2019**, vol. 7, pp. 39515-39527.

[10] Liu, G.L.; Gao, Z.K.; Chen, B.Y.; Fu, H.L.; Jiang, S.; Wang, L.P.; Wang, G. & Chen, Z.S. Extreme values of storm surge elevation in Hangzhou Bay. *Ships and Offshore Structures*, **2019**.

[11] Liu, G.; Chen, B.; Gao, Z.; Fu, H.; Jiang, S.; Wang, L.; Yi, K. Calculation of Joint Return Period for Connected Edge Data. *Water*, **2019**, vol. 11, pp. 300.

[12] Wang, L.; X. Xu, G. Liu, et al. A new method to estimate wave height of specified return period. Chin. *J. Ocean. Limnol*. **2017**, vol. 35, pp. 1002-1009.

[13] Wang, L.; Chen, B.; Chen, C., et al. Application of linear mean-square estimation in ocean engineering. *China Ocean Eng*, **2016**, vol. 30, pp. 149-160.

[14] Chen, B.; Zhang, K.; Wang, L., et al. Generalized Extreme Value-Pareto Distribution Function and Its Applications in Ocean Engineering. *China Ocean Eng*, **2019**, vol. 33, pp. 127-136.

[15] Chen, B.; Liu, G.; Wang, L., et al. Determination of water level design for an estuarine city. *J. Ocean. Limnol*. **2019**, vol. 37, pp. 1186-1196.

[16] Chen, B.; Kou, Y.; Zhao, D., et al. Calculations on stopping time and return period. *Nat Hazards*, **2020**, vol. 101, pp. 537-550.

[17] Wang, L.; Chen, B.; Zhang, J., et al. A new model for calculating the design wave height in typhoon-affected sea areas. *Nat Hazards*, **2013**,vol. 67, pp. 129-143.

[18] Chen, B.; Yang, Z.; Huang, S.; Du, X.; Cui, Z.; Bhimani, J., et al. Cyber-physical system enabled nearby traffic flow modelling for autonomous vehicles. 36th IEEE International Performance Computing and

Communications Conference. *Special Session on Cyber Physical Systems: Security, Computing, and Performance (IPCCC-CPS) IEEE*, **2017**.

[19] Escalante, H.J., et al. ChaLearn Joint Contest on Multimedia Challenges Beyond Visual Analysis: An overview. *2016 23rd International Conference on Pattern Recognition (ICPR), Cancun*, **2016**, pp. 67-73.

[20] Chen, B.; Liu, G.; Wang, L. Predicting Joint Return Period Under Ocean Extremes Based on a Maximum Entropy Compound Distribution Model. *International Journal of Energy and Environmental Science*, **2017**, vol. 2, no. 6, pp. 117-126.

[21] Chen, B.; Escalera, S.; Guyon, I., et al. Overcoming Calibration Problems in Pattern Labeling with Pairwise Ratings: Application to Personality Traits. Computer Vision-ECCV 2016 Workshops. *Springer, Cham*, **2016**, pp. 419-432.

[22] Ponce-L ópEZ, V.; Chen, B.; Oliu, M., et al. ChaLearn LAP 2016: First Round Challenge on First Impressions-Dataset and Results. Computer Vision-ECCV 2016 Workshops. *Springer, Cham*, **2016**, pp. 400-418.

[23] Liu, G.; Chen, B.; Wang, L., et al. Wave Height Statistical Characteristic Analysis. *Journal of oceanology and limnology*, **2019**, vol. 37, no. 2, pp. 448-460.

[24] Liu, X.; He, Y.; Fu, H.; Chen, B.; Wang, M.; Wang, Z. How Environmental Protection Motivation Influences on Residents' Recycled Water Reuse Behaviors: A Case Study in Xi'an City. *Water*, **2018**, vol. 10, pp. 1282.

[25] Song, J.; Feng, Q.; Wang, X.; Fu, H.; Jiang, W.; Chen, B. Spatial Association and Effect Evaluation of CO2 Emission in the Chengdu-Chongqing Urban Agglomeration: Quantitative Evidence from Social Network Analysis. *Sustainability*, **2019**, vol. 11, pp. 11-19.

[26] Jiang, S.; Lian, M.; Lu, C.; Ruan, S.; Wang, Z. & Chen, B. SVM-DS fusion based soft fault detection and diagnosis in solar water heaters. *Energy Exploration & Exploitation*, **2019**, vol. 37, no. 3, pp. 1125-1146.

[27] Xu, J.; Lei, B. Data Interpretation Technology of GPR Survey Based on Variational Mode Decomposition. *Applied Sciences*, **2019**, vol. 9, pp. 2017.

[28] Xu, J.; Wei, H. Ultrasonic Testing Analysis of Concrete Structure Based on S Transform. *Shock and Vibration*, **2019**.

[29] Xu, J., et al. Finite element simulation of prevention thermal cracking in mass concrete. *International Journal of Computing Science and Mathematics*, **2019**, vol. 10, no. 4, pp. 327-339.

[30] Zeng, Y.; Xie, Z.; Yu. Y.; Liu, S.; Wang, L.; Jia, B.; Qin, P.; Chen, Y. Ecohydrological effects of stream–aquifer water interaction: a case study of the Heihe River basin, northwestern China. *Hydrol Earth Syst Sc*, **2016**, vol. 20, pp. 2333-2352.

[31] Zeng, Y.; Xie, Z.; Zou, J. Hydrologic and Climatic Responses to Global Anthropogenic Groundwater Extraction. *J Climate*, **2017**, vol. 30, pp. 71-90.

[32] Zeng, Y.; Xie, Z.; Liu, S.; Xie, J.; Jia, B.; Qin, P.; Gao, J. Global land surface modeling including lateral groundwater flow. *J Adv Model Earth Sy*, **2018**, vol. 10, pp. 1882-1900.

[33] Gunaydin, K., Kabdali, M. Investigation of n-type breakwaters performance under regular and irregular waves. *Ocean Engineering*, **2007**, vol. 34, no. 7, pp. 1028-1043.

[34] Bulson, P. Bubble breakwaters with intermittent air supply, *The Dock and Harbour Aurhority*, **1963**, vol. 514, pp. 129-134.

[35] Dean, R.G., Dalrymple, R.A. Water wave mechanics for engineers and scientists. *World scientific publishing Co Inc*, **1991**, vol. 2.